

Supplementary Figure S1. Isolation of the Hmga2-GFP^{pos} PDAC sub-population from the *KPC^{colors}* mice and GFP^{pos} PDAC cells are a highly metastatic state.

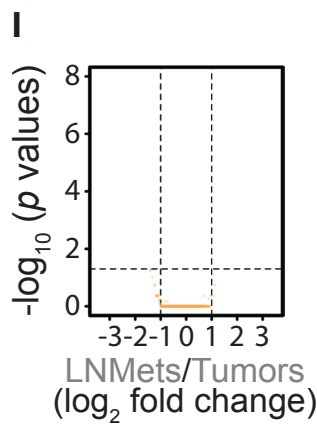
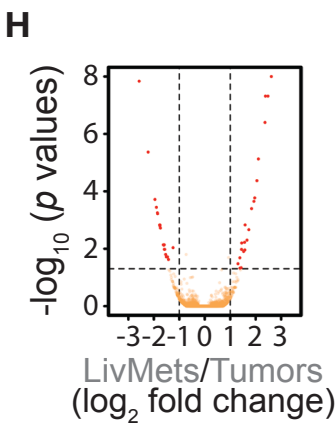
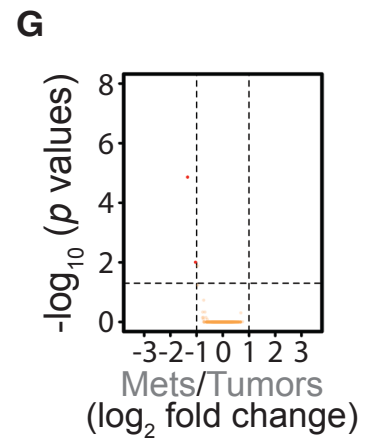
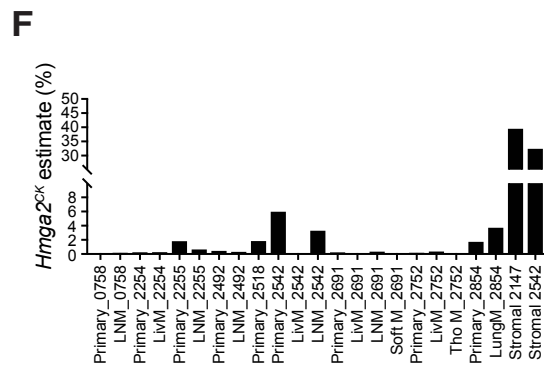
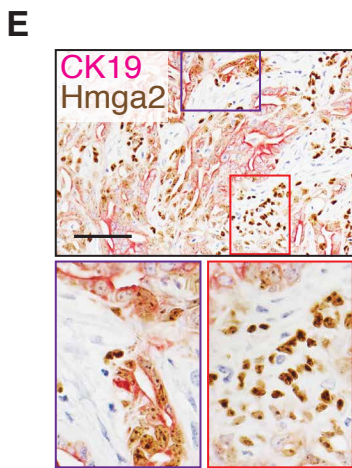
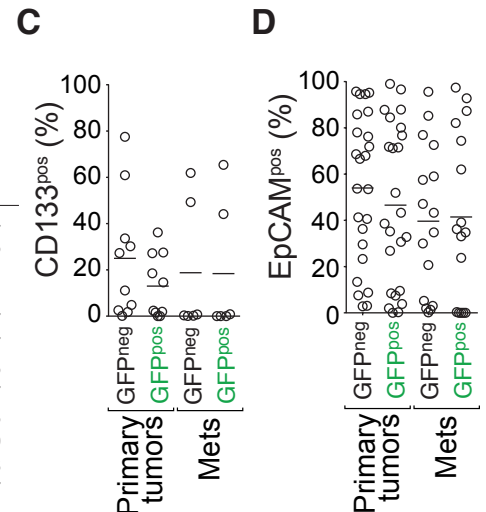
- (A) Immunohistochemistry for Hmga2 and GFP on adjacent sections of a primary PDAC (left) and liver metastasis (right) from a *KPC^{colors}* mouse. GFP and Hmga2 are co-expressed in a subset of cancer cells. Scale bars = 50 μ m.
- (B) HMGA2 protein expression quantified by immunohistochemistry on a human PDAC TMA predicts PDAC patient survival. Data from 166 patients. p-value < 0.006 by Log-rank test.
- (C) PDAC patients with tumors expressing higher a level of *HMGA2* have shorter overall survival. Data from 144 patients analysed by TCGA. p-value = 0.0016 by Log-rank test.
- (D) PDAC patients with tumors expressing a higher level of *HMGA2* have shorter overall survival. Data from 145 patients analysed by ICGC. p-value < 0.0001 by Log-rank test.
- (E) Representative images of adjacent sections stained for Hmga2, GFP, Tomato, and H&E from primary tumors from *KPC^{colors}* mice. Scale bars = 100 μ m.
- (F) Representative FACS gating used to isolate GFP^{pos} and GFP^{neg} pancreatic cancer cells from primary tumors from *KPC^{colors}* mice. FSC-A/SSC/FSC-H gating excludes cell doublets. DAPI^{neg} cells are viable cells. Lineage markers include CD45, CD31, F4/80, and Ter119.
- (G) Two representative western blots for concordant expression of Hmga2 and the Hmga2-GFP reporter in cancer cells from *KPC^{colors}* mice. Hsp90 shows loading.
- (H) PCR genotyping of purified GFP^{neg} and GFP^{pos} cells confirms minimal contaminating non-neoplastic cells (top) and documents *p53* LOH (bottom). *Hmga2^{CK/+}*, *Hmga2^{+/+}*, *p53^{+/+}* and *p53^{1loxP-R172H/+}* samples are positive and negative controls.
- (I) Pancreatic cancers in this model lose the wild-type *p53* allele, which leads to the stabilization of point-mutant *p53* encoded by the recombined *p53^{1loxP-R172H}* allele. To determine whether the Hmga2^{neg} and Hmga2^{pos} cells represent two distinct cancer cell states, we performed IHC for Hmga2 and *p53* on adjacent sections. Hmga2^{neg} and Hmga2^{pos} cells both have stabilized *p53* protein. Scale bars = 50 μ m.
- (J) GFP^{neg} and GFP^{pos} PDAC populations both have stabilized *p53* protein. GFP^{neg} and GFP^{pos} cancer cells were sorted by FACS as shown in (F). Hsp90 shows loading.
- (K) Purified GFP^{pos} PDAC cells have greater sphere forming ability. Number of cells plated is indicated. p-value < 0.04 by Wilcoxon matched-pair signed rank test.
- (L,M) Heterogeneous expression of Hmga2 in the metastases that form from GFP^{pos} PDAC cells in recipient mice. (L) Representative images of Tomato and Hmga2 IHC staining are shown. Tomato marks all cancer cells. Scale bars = 100 μ m. (M) Quantification of Hmga2 or Hmga2-GFP expression in the metastases that form in recipient mice after iv transplantation of GFP^{pos} or GFP^{neg} PDAC cells (Neg, <10% positive; Pos, >90% positive).

A

Sample	Cancer cell purity based on <i>Hmga2^{CK}</i> genotyping	Differential <i>Hmga2</i> protein confirmed by western	Differential sphere formation <i>in vitro</i>	Differential metastatic ability <i>in vivo</i>
2518T ^{GFP^{pos}}	>95%	Yes	n/d	Yes
2518T ^{GFP^{neg}}	>95%			
2542T1 ^{GFP^{pos}}	>95%	Yes	n/d	Yes
2542T1 ^{GFP^{neg}}	>85%			
2691T ^{GFP^{pos}}	>95%	Yes	Yes	n/d
2691T ^{GFP^{neg}}	>95%			
0784T2 ^{GFP^{pos}}	>95%	n/d	Yes	n/d
0784T2 ^{GFP^{neg}}	>95%			
2317T1 ^{GFP^{pos}}	>95%	Yes	Yes	n/d
2317T1 ^{GFP^{neg}}	>95%			
2689T1 ^{GFP^{pos}}	>95%	Yes	Yes	Yes
2689T1 ^{GFP^{neg}}	>85%			

B

Sample	<i>p53^{WT}</i> (Read#)	<i>p53^{R172H}</i> (Read#)	<i>p53^{R172H}</i> (%)	<i>Kras^{WT}</i> (Read#)	<i>Kras^{G12D}</i> (Read#)	<i>Kras^{G12D}</i> (%)
2518T ^{GFP^{pos}}	14	167	92.3	25	31	55.4
2518T ^{GFP^{neg}}	8	63	88.7	20	24	54.5
2542T1 ^{GFP^{pos}}	4	158	97.5	11	58	84.1
2542T1 ^{GFP^{neg}}	22	179	89.1	15	32	68.1
2691T ^{GFP^{pos}}	2	93	97.9	9	24	72.7
2691T ^{GFP^{neg}}	35	124	78.0	17	41	70.7
0784T2 ^{GFP^{pos}}	2	216	99.1	5	35	87.5
0784T2 ^{GFP^{neg}}	1	122	99.2	1	18	94.7
2317T1 ^{GFP^{pos}}	4	255	98.5	37	25	40.3
2317T1 ^{GFP^{neg}}	7	165	95.9	17	17	50.0
2689T1 ^{GFP^{pos}}	2	97	98.0	11	31	73.8
2689T1 ^{GFP^{neg}}	11	257	95.9	20	19	48.7



J

Gene Set (All curated)	NES	NOM p-value	FWER p-value
REACTOME_GLYCOSE_METABOLISM	-1.81	0.004	0.62
REACTOME_GLYCOLYSIS	-1.79	0.006	0.67
MOOHA_GLYCOLYSIS	-1.78	0	0.71
HSAIO_LIVER_SPECIFIC_GENES	-1.74	0.03	0.85
REACTOME_GLUONEOGENESIS	-1.71	0.01	0.94
MOOHA_GLUONEOGENESIS	-1.69	0.02	0.96

Supplementary Figure S2. Highly metastatic PDAC cells have a gene signature that is not enriched for CSC markers and distal PDAC metastases reveal minor gene expression changes related to glucose metabolism.

(A) General description of paired samples used for RNA-Seq. Sample purity was quantified by the ratio of unrecombined *Hmga2*^{CK} to WT *Hmga2* alleles through PCR genotyping. Efficacy of Hmga2 expression reported by GFP was validated by western blot analyses on sorted samples. Functional validation of dissociated GFP^{pos} and GFP^{neg} populations was conducted with *in vitro* sphere-forming assays and/or *in vivo* transplantation. n/d = no data available.

(B) All sequenced samples have lost the WT *p53* allele regardless of GFP/Hmga2 expression. Numbers of RNA-seq reads with mutant or wildtype *p53* and *Kras* alleles are shown. Please see Supplementary Methods for more details.

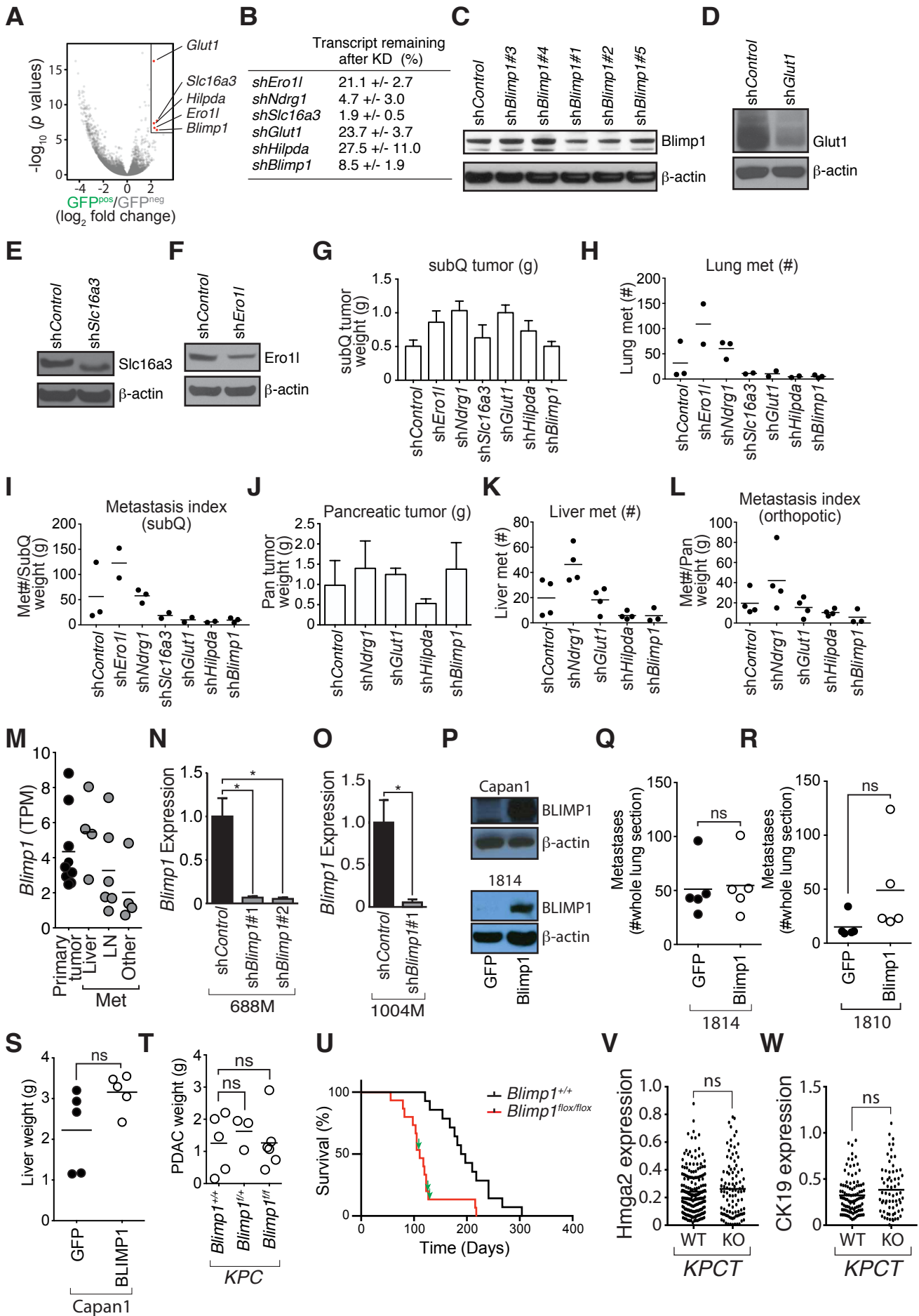
(C,D) Percent of GFP^{neg} and GFP^{pos} PDAC cells that express each surface marker quantified by flow cytometric analysis. Each dot is a tumor and the bar is the mean.

(E) Hmga2 expression marks a subset of moderately differentiated, CK19^{pos} (purple inset) and poorly-differentiated, CK19^{neg} (red inset) PDAC cells. Scale bars = 50 μ m.

(F) Estimated purities of purified Tomato^{pos} samples. To generate the standard curve, PCR amplicons of serially titrated *Hmga2*^{CK/CK} genomic DNA with *Hmga2*^{+/+} genomic DNA were quantified with densitometry. PCR amplicons of genomic DNA from indicated bulk sorted Tomato^{pos} lineage^{neg} samples were quantified with densitometry and the cell purities were estimated with the standard curve. Stromal samples (Stromal 2542 and Stromal 2854) were sorted as Tomato^{neg} lineage^{neg} cells and included as controls.

(G-I) Comparisons between bulk-sorted, Tomato^{pos} cancer cells from indicated anatomical locations. Horizontal dotted lines are adjusted p value = 0.05. Vertical dotted lines are log₂ fold change = +/- 1. Tumors, primary pancreatic tumors; LNMets, peritoneal or local lymph node metastases; LivMets, liver metastases. Mets, LNMets and LivMets combined.

(J) GSEA results of comparison between bulk primary pancreatic cancer cells and liver metastases. All curated gene sets (C2) were used, top 6 programs enriched in liver metastases are shown.



Supplementary Figure S3. Identification of top candidate pro-metastatic genes and interrogation of Blimp1 function in PDAC metastasis.

(A) Identification of candidate metastasis driver genes from *ex vivo* RNA-seq data analysis. We identified 5 top candidate genes with the cutoff of \log_2 fold change > 2 (GFP^{pos}/GFP^{neg}) and adjusted p value $< 10^{-6}$ by DESeq group-wise comparison.

(B) Top candidate genes (along with control gene *Ndr1*) were knocked down in a PDAC metastatic cell line 688M. Knockdown efficacies are shown as mean of remaining transcript quantified by qPCR +/- standard deviation of triplicated wells.

(C-F) Top candidate genes shown in (B) were knocked down in 688M cells cultured under hypoxia and the knockdown efficiency of Blimp1 (C), Glut1 (D), Slc16a3 (E), and Ero1l (F) are shown by western blot analyses. For *Blimp1*, hairpin sh*Blimp1*#1 was chosen for all other assays. β -actin shows loading.

(G-I) Assessments of the requirement for candidate genes in driving metastasis after subcutaneous (subQ) transplantation into immunocompromised NSG mice. (G) Weight (grams) of subQ tumors from transplanted 688M PDAC cell derivatives with indicated candidate (or control) genes knocked down by short hairpin RNA (shRNA). An shRNA against *GFP* is the negative control. Each dot is the average weight of the subQ tumors in one mouse and the bar is the average of all mice within that group. Mice were analyzed 24 days after transplantation. (H) Number of lung metastases from subQ transplantation. Each dot is a mouse and the bar is the mean. (I) Each dot is the number of lung metastases normalized to the average subQ tumor weight in that mouse.

(J-L) Assessments of the requirement for candidate genes in driving metastasis after orthotopic transplantation into the pancreas of NSG mice. (J) Weight of pancreatic orthotopic tumors derived from injected 688M PDAC cell derivatives with indicated candidate (or control) gene knockdown. Each dot is the weight of the orthotopic tumor in one mouse and the bar is the average of all mice. Mice were analyzed 24 days after transplantation. (K) Number of liver metastases from orthotopic transplantation. Each dot is a mouse and the bar is the mean. (L) Each dot is the number of liver metastases normalized to the orthotopic pancreatic tumor weight in that mouse.

(M) Expression of *Blimp1* (TPM) in bulk sorted cancer cells from primary and metastatic tumors of *KPCT* mice (not statistically significant by one-way ANOVA).

(N) qPCR confirmed efficient knockdown of *Blimp1* in the 688M PDAC cell line with 2 independent shRNAs. *, p-value < 0.05 by Student's t test.

(O) qPCR confirmed efficient knockdown of *Blimp1* in the 1004M PDAC cell line. *, p-value < 0.05 by Student's t test.

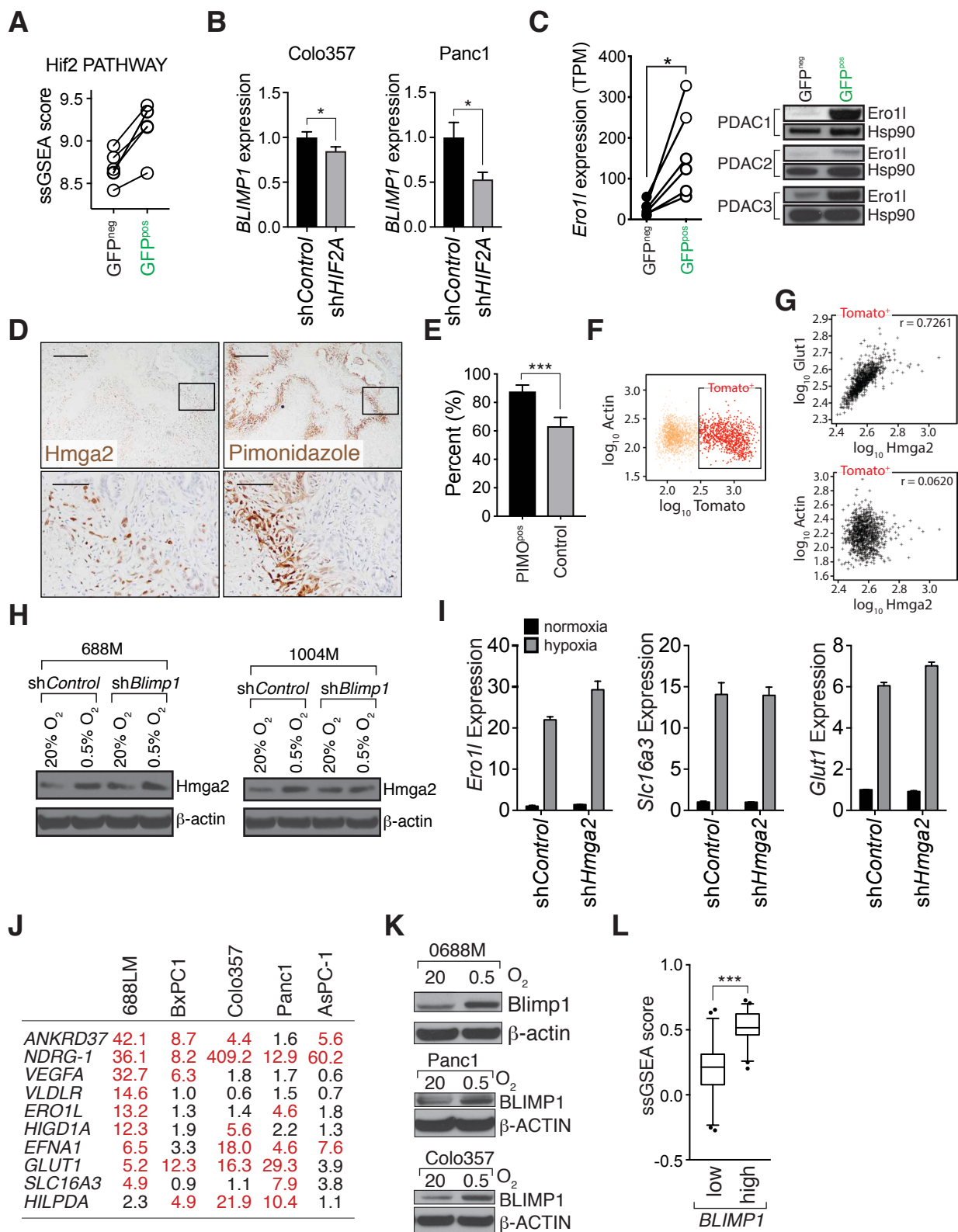
(P) Ectopic expression of BLIMP1 in the human PDAC cell line Capan1 (top panel) and the murine *Blimp1*-deficient PDAC cell 1814 (bottom panel).

(Q-S) Ectopically expressed BLIMP1 is not sufficient to enhance PDAC metastasis. Number of lung metastases (Q,R) and total liver weights (S) were quantified following subcutaneous (Q,R) and i.v. (S) transplantation of indicated PDAC cell lines with or without Blimp1 or BLIMP1 expression. ns, not statistically significant by Student's t test.

(T) *Blimp1* deficiency does not alter primary PDAC size in *KPC* mice. ns, not statistically significant by Student's t test.

(U) Survival curve of *KPTC;Blimp1^{+/+}* and *KPTC;Blimp1^{fl/fl}* mice. Green arrows indicate mice in the *KPTC;Blimp1^{fl/fl}* cohort that had metastases. p = 0.0001 by log-rank test.

(V,W) *Blimp1* deficiency in the *KPCT* mice does not change the expression of Hmga2 or CK19. Quantification of the brown pixels per field by FIJI.



Supplementary Figure S4. Hmga2^{positive} PDAC areas overlap with hypoxic areas and Hmga2 protein is slightly induced by hypoxia but not critical to the expression of hypoxia-induced target genes.

(A) Hmga2/GFP^{pos} cancer cells are enriched for the “PID_HIF2PATHWAY” geneset. Single-sample GSEA (ssGSEA) scores for each sorted sample are plotted. Adjusted p value = 7.2×10^{-5} with an FDR = 0.1.

(B) *BLIMP1* expression under hypoxia (0.5% O₂ for 24 hours) is partially dependent on *HIF2A* in human PDAC cell lines. *BLIMP1* level was quantified by qPCR.

(C) GFP^{positive} PDAC cells have higher expression of the known hypoxia/Hif target *Ero1l*, at both the transcript (TPM, left) and protein (western blot analysis, right) levels. Hsp90 shows loading.

(D,E) Pimonidazole (PIMO)-defined hypoxic areas are enriched for Hmga2-expressing cancer cells. (D, bottom panels) High magnification images show areas bordering regions that are necrotic. Top scale bars = 300 μ m. Bottom scale bars = 60 μ m. (E) PIMO^{pos} and total areas (control) were quantified for Hmga2 expression by counting the number of areas with (count as 1) or without Hmga2 (count as 0) expression on multiple nearby sections (n = 5). ***, p < 0.0005 by Student's t test.

(F,G) Hmga2^{pos} areas are highly enriched with canonical hypoxia target Glut1 measured by AT ribbon arrays. All interrogated markers, including Hmga2, Glut1, and Actin, were stained and imaged on the same resin-embedded tissue section, which allowed accurate quantification of the correlation between stained markers. (F) Processed images were parsed into 90x90 (100x100 nm) pixel squares and the relationship between measured Tomato and Actin intensities (log₁₀) is shown. For the quantification of how well any two markers correlate within cancer cells, we focused on Tomato^{pos} regions where cancer cells are located. (G) Hmga2 expression is highly correlated with Glut1 expression but not with Actin.

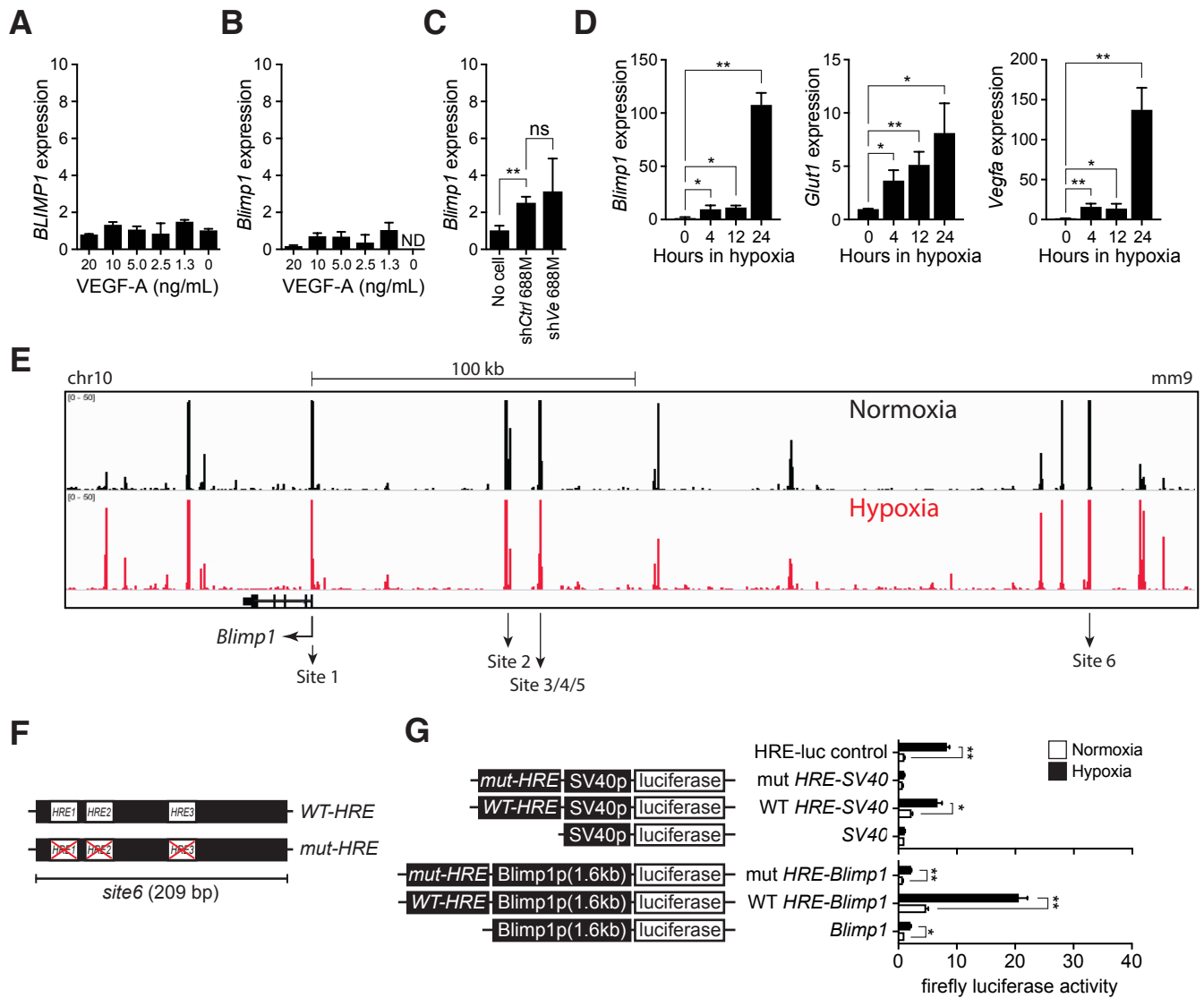
(H) Hmga2 protein is slightly upregulated under hypoxia. Indicated murine PDAC cell lines were cultured in 20% (normoxia) or 0.5% O₂ (hypoxia) before western blot analyses for Hmga2 protein. For each cell line, both control and *Blimp1* knockdown cells were included in order to assess the impact of *Blimp1* knockdown on Hmga2 expression. β -actin shows loading.

(I) *Hmga2* knockdown does not greatly change the induction of hypoxia target genes. The levels of hypoxia target gene *Ero1l*, *Slc16a3*, and *Glut1* in 688M PDAC cells cultured under normoxia and hypoxia were quantified by qPCR.

(J) Quantification of genes up-regulated in the indicated cell lines when cultured under hypoxic condition. Expression was quantified by qPCR and the expression of each gene under hypoxia normalized to the expression level under normoxia is shown (0.5% O₂ for 24 hours).

(K) Hypoxia (0.5% O₂ for 24 hours) induces *Blimp1* protein expression in the mouse PDAC cell line 688M and two human PDAC cell lines. β -actin shows loading.

(L) *BLIMP1* expression correlates with hypoxia-induced gene expression programs in human PDAC. Single-sample GSEA (ssGSEA) scores for the GSEA process GROSS_HIF1A_TARGETS_UP were calculated for each patient in the TCGA PDAC dataset. Tumors with *BLIMP1* expression within the top quartile (high) and bottom quartile (low) are shown. ***, FDR < 0.0005.



Supplementary Figure S5. Hypoxia-induced *Blimp1* expression is linked to functional HRE motifs 240 kb upstream of its transcription start site.

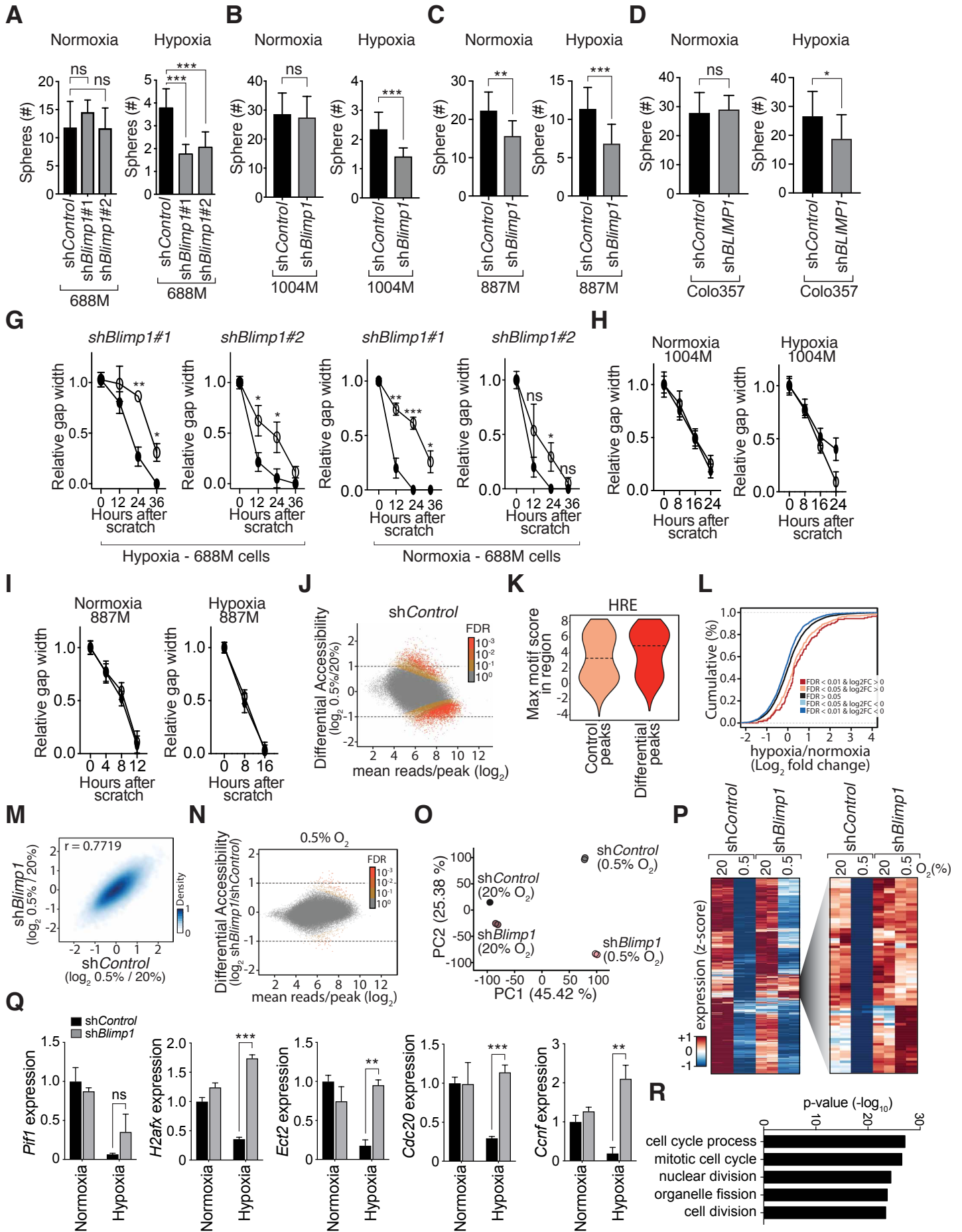
(A,B) VEGF-A does not change *Blimp1* expression. Panc1 (A) and 688M PDAC cells (B) were treated with indicated concentrations of recombinant VEGF-A for 3 days under normoxia and *Blimp1* expression was quantified by qPCR. ND, not detected.

(C) Conditioned medium derived from 688M cells cultured under hypoxia only slightly induced *Blimp1* expression. 688M PDAC cells with control (shCtrl) or *Vegfa* (shVe) knockdown were used. **, p value < 0.005 by student's t test. ns, not statistically significant.

(D) The kinetics of hypoxia-induced *Blimp1* expression are comparable to those of canonical Hif1 target genes. *Blimp1* (left), *Glut1* (middle), and *Vegfa* (right) expression was quantified by qPCR at indicated hours cultured under hypoxia. *, p value < 0.05; **, p value < 0.005 by Student's t test.

(E) ATAC-Seq tracks of 688M cells cultured under normoxia or hypoxia where peaks assigned to the *Blimp1* locus are shown. Peaks with high-score HREs (site1-6) are highlighted.

(F,G) *Site6* has three HREs that impart strong hypoxia responsiveness to a 1.6kb *Blimp1* promoter. The schematic of wildtype and HRE-disrupted *site6* is shown (F). The wildtype 209 bp-long *site6* was subcloned into a luciferase reporter plasmid and mutagenized at all three HRE sites (left, G). Both a SV40 promoter and a 1.6 kb *Blimp1* promoter were used to measure the function of *site6* under hypoxia. (right, G) Representative results of 1004M cells transfected with indicated reporters and cultured under normoxia or hypoxia are shown.



Supplementary Figure S6. Blimp1 may contribute to migratory and clonal growth ability and is critical for a subset of hypoxia-induced gene expression changes that are independent of changes in chromatin accessibility.

(A-D) *Blimp1* influences sphere formation of cells cultured in serum-free medium. PDAC cell line 688M (A), 1004M (B), 887M (C), and Colo357 (D) were cultured under normoxia or hypoxia for 3 days before assessing sphere formation in low-attachment plates.

(E) Timeline for the scratch assay under hypoxia. Subconfluent (~80% confluent) 688M cells were cultured for 24 hours under hypoxia (0.5% O₂) before scratch at 0 hour and assayed under normoxia at indicated time points.

(F,G) *Blimp1* knockdown with 2 different shRNAs under both normoxia and hypoxia reduces the migration ability of 688M PDAC cells measured by scratch assay. (F) Representative images of 688M cell migration with control and *Blimp1* knockdown with two different shRNAs. (G) Each point is the mean +/- SD of triplicate wells. **, p < 0.005; *, p < 0.05 by Student's t test.

(H,I) *Blimp1* knockdown does not change the migratory ability of 1004M (G) and 887M (H) PDAC cells measured by scratch assay. Each point is the mean +/- SD of triplicate wells.

(J) Hypoxia (0.5% O₂ for 24 hours) in shControl cells induces global changes in chromatin accessibility.

(K) Hypoxia-response element (HRE) motif enrichment in differentially accessible regions compared to the control regions. Control regions were constitutively open peaks. Motif scores were derived with Homer's annotatePeaks.pl command.

(L) The status of chromatin regions near TSS is highly correlated with gene expression changes induced by hypoxia. Genes that are associated with newly open chromatin regions (within 1000 bp from the TSS, log₂FC > 0) tend to be induced under hypoxia, while genes that are associated with newly closed regions (log₂FC < 0) appear to be suppressed by hypoxia. Cumulative log₂ fold change of shControl 688M cells cultured under hypoxia over normoxia is shown. p < 0.0001 by Kruskal-Wallis test.

(M) *Blimp1* knockdown has a minimum impact on chromatin accessibility induced under hypoxia. Hypoxia-induced changes in chromatin accessibility (log₂ fold change) in shControl cells (X axis) are highly correlated with those induced in sh*Blimp1* cells (Y axis). Correlation is measured by Pearson correlation coefficient r.

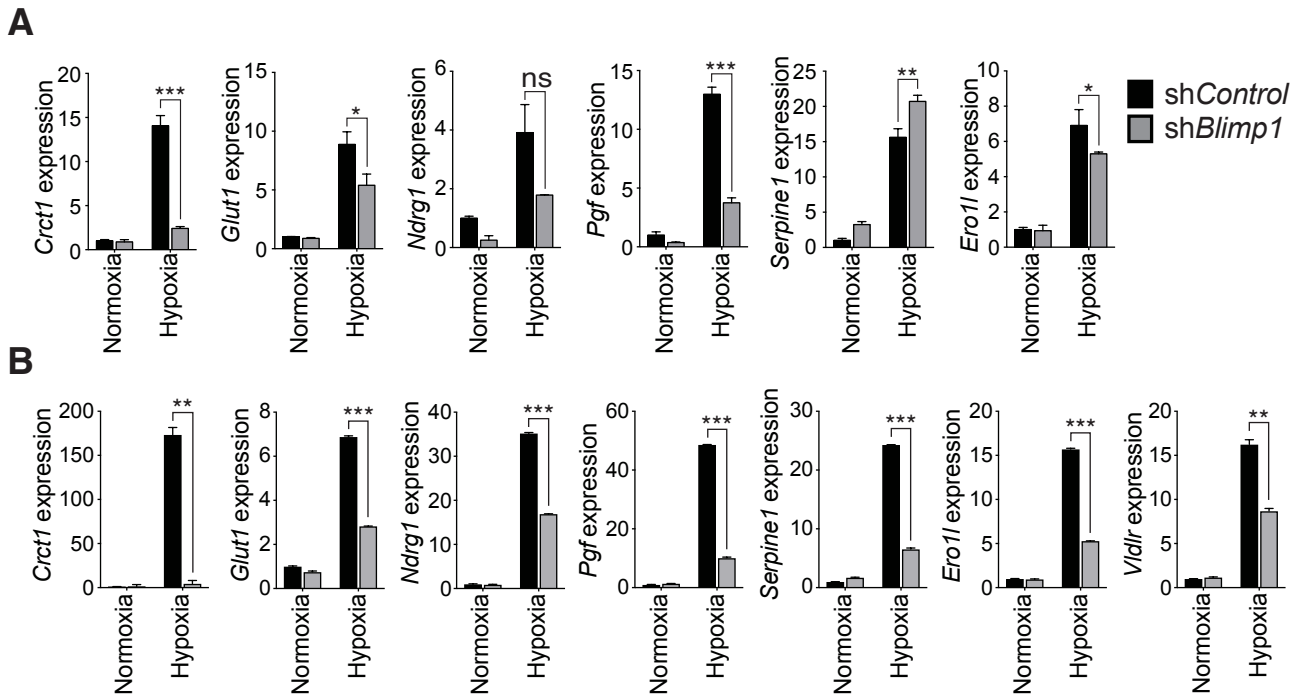
(N) *Blimp1* knockdown induces minimum changes of chromatin accessibility under hypoxia.

(O) Principle component analysis (PCA) of gene expression (TPM) from RNA-seq of all samples as described in Figure 5A. Principle component 1 versus 2 with proportions (%) of variance shown within brackets. PCA calculated with r package "prcomp".

(P) About 12% of hypoxia-suppressed genes requires *Blimp1* for their full suppression and were at least 2-fold less suppressed by hypoxia upon *Blimp1* knockdown. Right panel, heatmap highlighting genes within this category.

(Q) Validation of indicated hypoxia-repressed, *Blimp1*-dependent target genes by qPCR in the 688M PDAC cell line. Control knockdown (black bar) and *Blimp1* knockdown (gray bar) 688M cells were cultured under hypoxia or normoxia for 24 hours. ***, p < 0.0005; **, p < 0.005; *, p < 0.05 by Student's t test. Mean +/- standard deviation of triplicated wells is shown.

(R) GO term analysis of hypoxia-suppressed, *Blimp1*-dependent genes highlighted in (P).



C Accessible regions linked by 500 kb proximity. Target: 2189 regions, Background: 2209 regions

Motif	log(p-val.)	q-val. (Benjamini)	% Target Regions	% Background Regions
IRF1(IRF)/PBMC-IRF1-ChIP-Seq(GSE43036)/Homer	-10.54	0.0085	4.52%	2.95%
IRF2(IRF)/Erythroblas-IRF2-ChIP-Seq(GSE36985)/Homer	-9.465	0.0085	3.75%	2.34%
CEBP:CEBP(bZIP)/MEF-Chop-ChIP-Seq(GSE35681)/Homer	-8.559	0.0154	3.47%	2.21%
AARE(HLH)/mES-cMyc-ChIP-Seq/Homer	-7.913	0.0235	3.20%	2.03%
GATA3(Zf),DR4/iTreg-Gata3-ChIP-Seq(GSE20898)/Homer	-7.419	0.0321	2.10%	1.22%

D

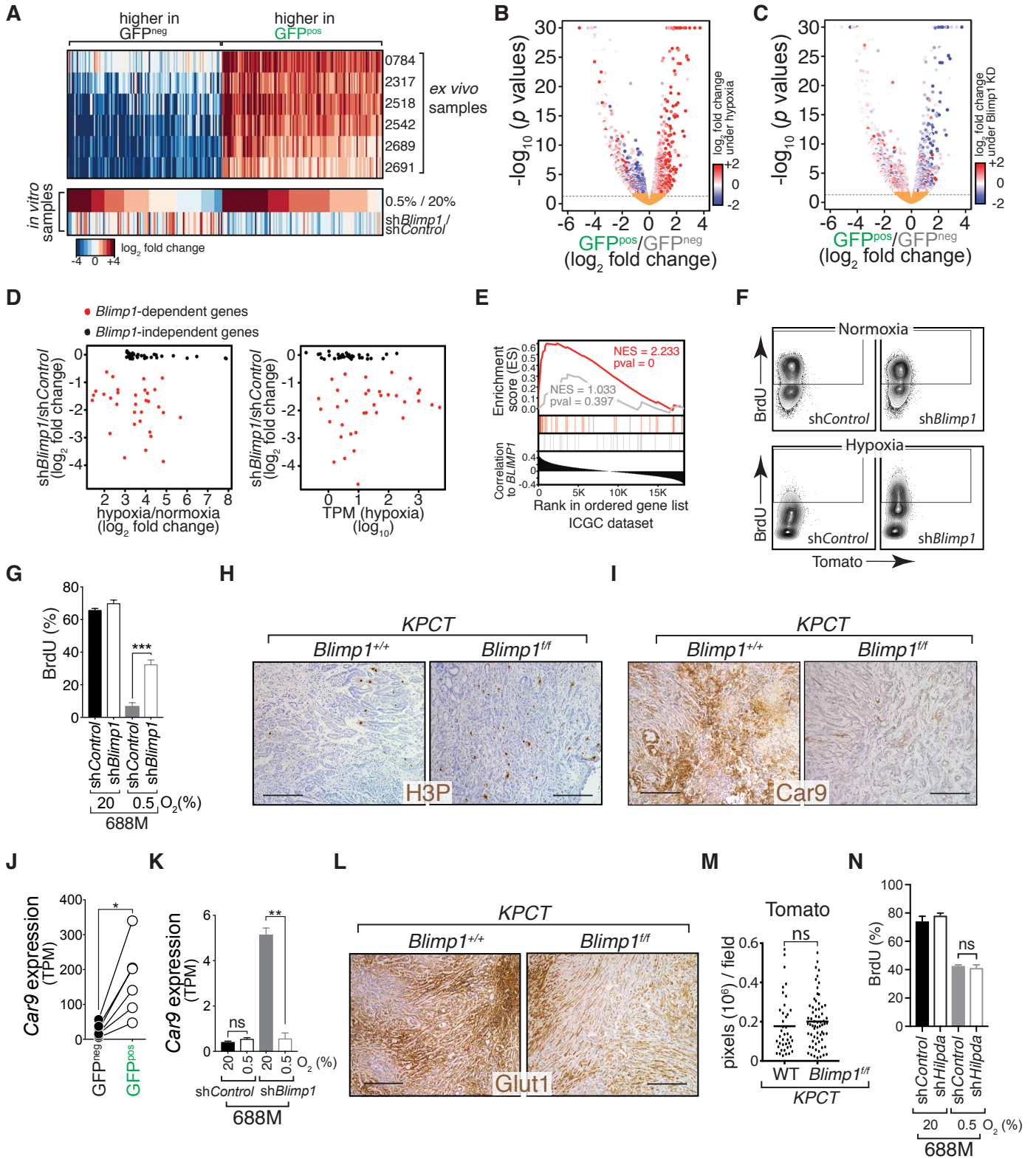
	BLIMP1-dependent	BLIMP1-independent	Motif logo
Gene number	41	41	
Associated Peaks	2189	2209	
Peaks with <i>BLIMP1</i> Motif	102	97	
Peaks with <i>IRF1</i> Motif	29	10	
Peaks with <i>IRF2</i> Motif	20	5	

Supplementary Figure S7. Blimp1 regulates a subset of hypoxia-induced genes.

(A,B) Validation of the hypoxia induction and *Blimp1* dependence of the indicated genes in the 1004M (A) and 688M (B) PDAC cell lines. *Control* (black bar) and *Blimp1* knockdown (gray bar) cells were cultured under hypoxia or normoxia for 24 hours before qPCR analyses. ***, $p < 0.0005$; **, $p < 0.005$; *, $p < 0.05$ by Student's t test. Mean \pm standard deviation of triplicate wells is shown.

(C) Motif enrichment results for accessible regions linked to *Blimp1*-dependent genes (Target peak set, $n = 2189$) compared to *Blimp1*-independent genes (Background peak set, $n = 2209$) from gene lists described in Figure 6B-6C. Accessible regions were merged across all samples ($n = 8$, Figure 5A). Accessible region-gene linking was done using a distance cutoff of 500 kb on either side of the gene's transcription start site, with nearest-gene used as the criterion for disambiguating links for regions within 500 kb of two genes (see Supplementary Methods for detail). Q-values are based on the HOMER enrichment calculation with Benjamini multiple hypothesis correction. P-values shown are estimated by bootstrapping 1000 permutations of the target and background peak labels using HOMER log p-values. Top 5 hits from the HOMER known motif result are shown.

(D) Numbers and the motif logos of indicated motifs found in target and background regions described in (C). The numbers and motif logo of *BLIMP1* motif are shown in comparison. Note the similarity between the IRF1/2 and *Blimp1* motifs.



Supplementary Figure S8. *Blimp1* is required for hypoxia-induced cell cycle arrest and the expression of metastasis modulators.

(A) Many of the genes that are differentially expressed between GFP^{pos} and GFP^{neg} cancer cells (left panel) are modulated under hypoxia. For comparison, hypoxia-induced fold change (\log_2 -converted ratio of shControl-0.5% O₂ / shControl-20% O₂, 7th row) and *Blimp1* knockdown-induced fold change (\log_2 -converted ratio of sh*Blimp1*-0.5% O₂ / shControl-0.5% O₂, 8th row) in gene expression of the same set of genes are shown. Heatmap reveals \log_2 fold change in gene expression of GFP^{pos} over GFP^{neg} cancer cells (*ex vivo* samples). Gene list for the heatmap was derived from DESeq2-called differentially expressed genes (FDR < 0.001 and absolute \log_2 fold change > 1) between GFP^{pos} and GFP^{neg} cancer cells, which was further trimmed down for genes with low expression levels from *in vitro* dataset.

(B,C) Volcano plots of the *ex vivo* dataset (sorted GFP^{pos} versus GFP^{neg} cancer cells) color-coded to reflect the \log_2 fold change under hypoxia (0.5%-shControl / 20%-shControl, B) or the \log_2 fold change upon *Blimp1* knockdown under hypoxia (0.5%-sh*Blimp1* / 0.5%-shControl, C).

(D) Hypoxia-induced fold change (left) and expression under hypoxia (TPM, right) of 41 *Blimp1*-dependent (red) and *Blimp1*-independent, hypoxia-induced genes. Y axis shows changes induced by *Blimp1* knockdown under hypoxia (\log_2 fold change of sh*Blimp1* 0.5% O₂ / shControl 0.5% O₂).

(E) BLIMP1 expression correlates with a subset of hypoxia-induced genes in human PDAC. All genes from the ICGC PDAC dataset are ranked by their correlation with BLIMP1 expression (Pearson r) and enrichments of 36 BLIMP1-dependent (red) and 36 BLIMP1-independent (grey), hypoxia-induced genes are shown. NS, enrichment score; NES, normalized enrichment score; pval, nominal p-value.

(F,G) *Blimp1* knockdown partially relieved hypoxia-induced cell cycle arrest. 688M cells were cultured under 20% or 0.5% O₂ for 24 hours and labelled with bromodeoxyuridine (BrdU). BrdU incorporation was quantified by FACS. Representative FACS plots (F) and quantification of the mean +/- SD of triplicate wells (G) are shown. ***, p-value < 0.0005 by Student's t test.

(H) *Blimp1* deficiency in *KPCT* mice increases PDAC cell proliferation. Proliferation was measured by IHC for phospho-histone 3 (H3P) and representative images are shown (N = 3 mice per group). Scale bars = 200 μ m.

(I) *Blimp1* deficiency in *KPCT* mice significantly reduces Car9 expression by IHC. Representative IHC images of Car9 expression in PDAC in mice of the indicated genotypes are shown. Scale bars = 200 μ m.

(J) Expression (TPM) of *Car9* in purified GFP^{pos} and GFP^{neg} PDAC cells from the *KPC^{colors}* mice. *, p-value < 0.05 by Student's t test.

(K) *Blimp1* knockdown significantly reduced hypoxia-induced *Car9* expression (TPM). **, p-value < 0.005. ns, not statistically significant by Student's t test.

(L) *Blimp1* deficiency in *KPCT* mice significantly reduces Glut1 expression by IHC. Representative IHC images of Glut1 expression in PDAC in mice of the indicated genotypes are shown. Scale bars = 200 μ m.

(M) Comparison of Tomato expressed in PDAC derived from the control *KPTC;Blimp1^{+/+}* (n = 2) and *KPTC;Blimp1^{fl/fl}* (n = 2) mice by IHC. Tomato staining in both cohorts of mice with distinct *Blimp1* genotypes serves as control for the quantifications of IHC staining. Areas with brown staining were quantified by FIJI. ns, not statistically significant by Student's t test.

(N) *Hilpda* knockdown does not change the level of hypoxia-induced cell cycle arrest. 688M cells were cultured under 20% or 0.5% O₂ for 24 hours and BrdU incorporation was quantified by FACS. Mean +/- SD of triplicate wells is shown. ns, not statistically significant.